Revealing Factors Influencing the Operational Stability of Perovskite Light Emitting Diodes

*Jonathan H. Warby, Bernard Wenger, Alexandra J. Ramadan, Robert D. J. Oliver, Harry C. Sansom, Ashley R. Marshall and Henry J. Snaith**

Clarendon Laboratory, Department of Physics, University of Oxford, Oxford OX1 3PU, UK

Abstract

Light emitting diodes (LEDs) made from metal halide perovskites have demonstrated external electroluminescent quantum efficiencies (EQE_{EL}) in excess of 20%. However, their poor operational stability, resulting in lifetimes of only tens to hundreds of hours, needs to be dramatically improved prior to commercial use. There is little consensus in the community upon which factors limit the stability of these devices. Here, we investigate the role played by ammonium cations on the operational stability. We vary the amount of phenylethylammonium bromide, a widely used alkylammonium salt, we add to a precursor solution of $CsPbBr_3$ and track changes in stability and EQE_{EL}. We find that while phenylethylammonium bromide is beneficial in achieving high efficiency, it is highly detrimental to operational stability. We investigate material properties and electronic characteristics before and after degradation and find that both a reduction in the radiative efficiency of the emitter and significant changes in current-voltage characteristics explain the orders of magnitude drop in the EQE_{EL} which we attribute to increased ionic mobility. Our results suggest that engineering new contacts and

further investigation into materials with lower ionic mobility should yield much improved stability of perovskite LEDs.

Keywords

perovskite, light-emitting diode, 2D/3D, stability, $CsPbBr_3$, efficiency, degradation

Metal halide perovskite semiconductors have emerged in recent years as a class of materials with enormous potential for diverse optoelectronic applications. They have been intensively studied for photovoltaic applications where power conversion efficiencies in excess of 25% have recently been reported.[1] The perovskite photovoltaic community rapidly garnered interest as efficiencies in excess of 10% were reported in 2012,[2] after which the efficiency rapidly rose. As gains in efficiency became more incremental, the instability of the cells under operational conditions was confronted and recent reports show stabilities of 1000s of hours.[3]

Following a few years after the solar cell breakthroughs of 2012, light emitting diodes (LEDs) based on ABX_3 metal halide perovskites were reported.[4] The research field has been following a similar trend to perovskite photovoltaics where initial modest efficiencies have rapidly improved.[5] Currently there are several reports of perovskite LEDs with an external electroluminescence quantum efficiency (EQE_{EL}) in excess of 20%, which is comparable with state of the art organic LEDs.[6–9] However, the operational stability of perovskite LEDs is currently poor; state-of-the-art devices only able to operate for a few hours, or a few hundred hours in the best case.[9] These lifetimes fall orders of magnitude short of those in organic LEDs (OLEDs), which can operate for tens of thousands of hours, limiting the scope for commercial use. Now that high efficiencies have been demonstrated, the poor stability needs to be more urgently addressed, and will "gate" whether perovskites will have a future in the LED industry.

Over the last few years, high efficiency perovskite LEDs have been most often made by *in situ* generation of nanocrystals in a film (where a ligand is added in excess to the stoichiometric ABX_3 perovskite) [10] or through the formation of quantum well heterostructures (often referred to as "2D/3D" compositions).[11] In both cases, bulky ammonium cations are used to improve the optoelectronic properties of the material by direct chemical passivation, increased dielectric confinement, carrier funnelling and reduction in grain size, all which encourage efficient radiative bimolecular recombination.[11–13] Despite the widespread use of bulky ammonium cations there has been very little study into their effect on stability.

In this work we investigate the effect of the composition of the emissive layer on the stability of perovskite LEDs by systematically varying the amount of excess phenylethylammonium bromide (PEABr) (structure Fig. S1 b) which we add to our control precursor solution of cesium lead tri-bromide ($CsPbBr_3$). PEABr has been widely used for high efficiency LEDs in the literature for both nanocrystalline films and 2D/3D compositions [11,13,14] We demonstrate that addition of PEABr into the precursor solution is an effective strategy to improve the efficiency of perovskite LEDs where we observe 50 fold improvement in EQE_{EL} from 0.24% for $CsPbBr_3$ to over 12.1% for our optimised composition. Despite this excellent improvement in efficiency, we find that the LEDs containing PEABr are much less stable than those which do not. We find that two factors strongly govern the instability: i) a large drop in the radiative efficiency of the emitter layer and, ii) most significantly, the emergence of a charge injection barrier in the LEDs which we postulate leads to charge imbalance in the device.

Results and Discussion

We choose $CsPbBr_3$ as our emitter material, so that phenylethylammonium (PEA) is the only organic cation in our system.[15] We begin our investigation by fabricating films of $CsPbBr_3$ *via* spin-coating. Using scanning electron microscopy (SEM) (shown in Fig. S1a), we find that for $CsPbBr_3$ we obtain a non – continuous film with crystallites that are a few hundred nanometres

in size. We then fabricate films by adding increasing excess of phenylethylammonium bromide (PEABr) to the stoichiometric solutions of $CsPbBr_3$ precursors. We add the small molecule 18-crown-6 to improve both the morphology and optoelectronic quality of the polycrystalline films, as previously reported by Ban *et al.*;[14] 18-crown-6 is used at a concentration of 4 mg/mL for all films in this study unless stated otherwise. We show SEM images of the films in Figure S1b, and observe a significant decrease in grain size as we increase the amount of PEABr. Crystallites are typically < 50 nm for the $(PEABr)_{0.2}CsPbBr_3$ films and for the $(PEABr)_{0.4}CsPbBr_3$ and $(PEABr)_{0.6}CsPbBr_3$ individual grains are not easily resolved. We note that the compositions which we refer to reflect the molar ratio of PEABr to $CsPbBr_3$ in the starting solutions. They do not represent the crystal phase in the as-crystallised film, which we discuss in detail later on.

Next, we assess the optoelectronic properties and quality of the films. We begin by characterising the photoluminescence (PL, Fig. 1a) and UV-Visible absorption (UV-Vis, Fig. 1b) spectra of the films. We present photographs of the same films under visible and UV illumination in Fig. 2d.i. and 2.d.ii. For the $CsPbBr_3$ films we observe an excitonic absorption feature peaked at 515 nm. As the molar ratio of PEABr is increased we observe significant changes in both the absorption and photoluminescence spectra. We observe a blue-shift of the absorption onset which we hypothesise to be due to quantum confinement of the carriers within the emissive domains. There is also a broadening of the excitonic absorption (see Supplementary Note 1 for further discussion). We observe distinct absorption features in our (PEABr)1.0CsPbBr3 sample at 435 and 460 nm which are likely due to the presence of n=2 and n=3 Ruddlesden-Popper phases of the formula $PEA_2Cs_{n-1}Pb_nBr_{3n+1}$.[16] It appears that our film fabrication procedure favours the formation of 3D over 2D phases until we reach a critical point where there is high amount of PEABr. Steady state photoluminescence spectra show a blue-shift in the emission peak and broadening of the spectrum with increasing amounts of

PEABr (see Supplementary Note 1). This is consistent with our hypothesis of confinement of the carriers, which is typically observed in $CsPbBr_3$ nanocrystals below 15 nm.[17]

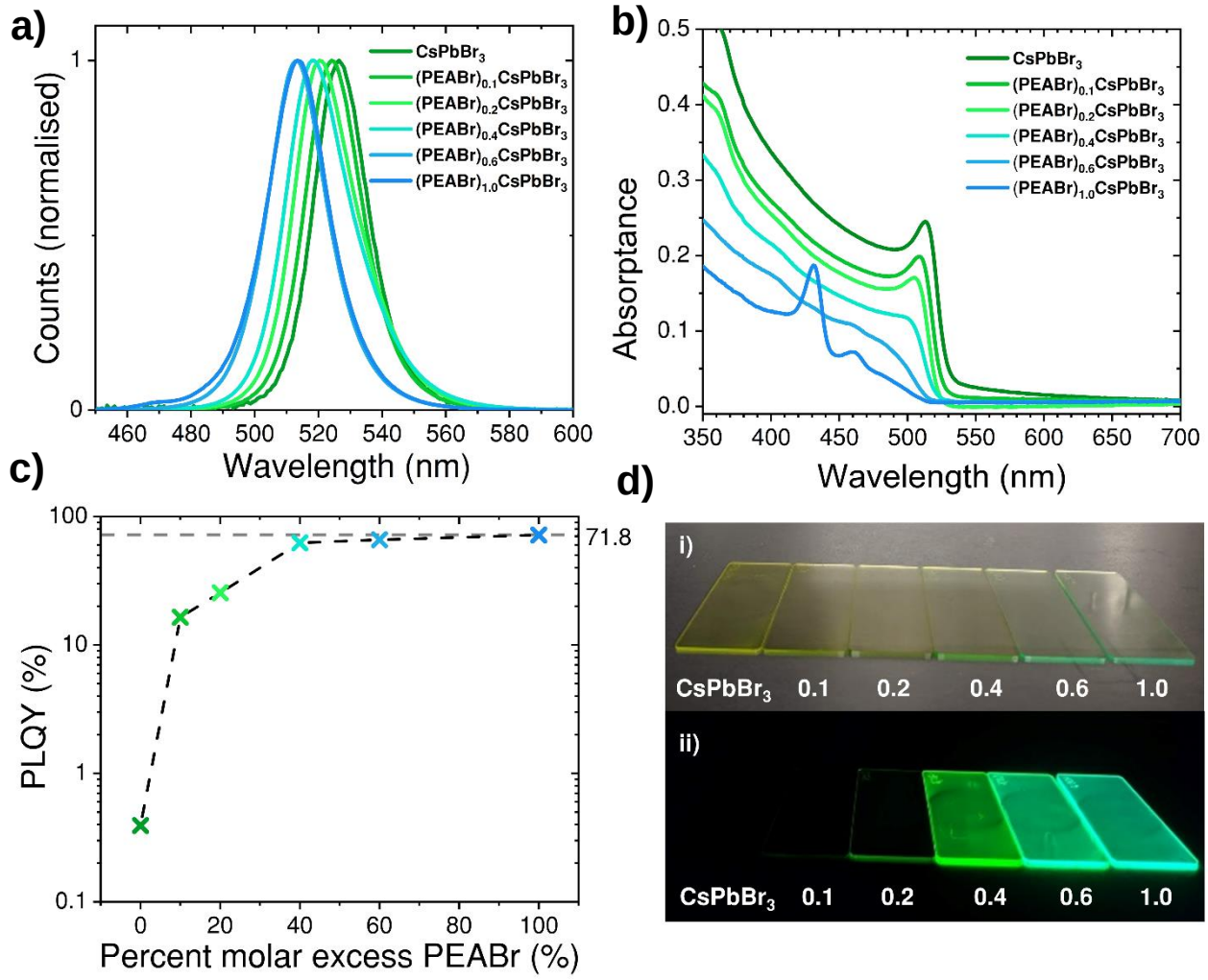

Figure 1. Photophysical characterisation of PEABr/$CsPbBr_3$ films: a) Normalised photoluminescence spectra of $CsPbBr_3$ with increasing molar excess of PEABr; b) Absorptance data of $CsPbBr_3$ with increasing molar excess of PEABr; c) Photoluminescent quantum yield of $CsPbBr_3$ with increasing molar excess of PEABr; d) i) Photograph of films used for characterisation under ambient lighting in glovebox, numbers indicate molar fraction *i.e.* 0.1 = $(PEABr)_{0.1}CsPbBr_3$, ii) Photograph of corresponding films under 365 nm UV light in glovebox.

From SEM, UV-Vis and steady state PL we conclude that, as we increase the concentration of PEABr, we are forming nanocrystalline domains of decreasing size of $CsPbBr_3$, which then begins to form 2D structures when the precursor has the composition $(PEABr)_{1.0}CsPbBr_3$. This agrees with other reports which use excess PEABr as an additive into ABX_3 precursor solutions, and show the formation of nanocrystalline domains.[10,14] This is further corroborated by X-ray diffraction (XRD) data $(PEABr)_{0.4}CsPbBr_3$, which shows the same diffraction peaks as $CsPbBr_3$ with no reflections at lower angles, which we would expect from 2 dimensional phases (Fig. S3 a-c). We fit the (101) diffraction peak centred at 15.2° and found that there is a three-fold broadening of the peaks in our $(PEABr)_{0.4}CsPbBr_3$ films which is consistent with a large reduction in particle size (Fig S3 d). If we assume the domains are spherical, we find through Scherrer broadening analysis that this corresponds to an average domain diameter of 47 nm for $CsPbBr_3$, reducing to 15 nm for the $(PEABr)_{0.4}CsPbBr_3$ films.

We investigate the impact of PEABr concentration on the photoluminescence quantum yield (PLQY) of the films (Fig. 2c), which is the ratio between the photons emitted to the photons absorbed. PLQY is a critical parameter for an emitter in an LED since it represents the maximum possible value for the EQE_{EL} if all other losses are accounted for in the device.[18,19] We find that at an irradiance of 93 mW/cm^2 (at 405 nm), addition of PEABr improves the PLQY from 0.4 % for our neat $CsPbBr_3$ film to 71.8 % for the $(PEABr)_{1.0}CsPbBr_3$ film (see Table 1 for further details). This is among the highest values reported for a perovskite thin film, which is additionally smooth with no enhanced scattering or optical out-coupling structures.[11,20]

Perovskite Composition	**PL Peak (nm)**	**PLQY (%)**	**FWHM (nm)**	**PL Stability – I/I_0 after 300 s**
$CsPbBr_3$	526	0.4	21.2	1.26
$(PEABr)_{0.1}CsPbBr_3$	524	16.4	22.4	0.76

$(PEABr)_{0.2}CsPbBr_3$	520	25.5	25.3	0.58
$(PEABr)_{0.4}CsPbBr_3$	518	62.3	26.8	0.84
$(PEABr)_{0.6}CsPbBr_3$	512	66.0	23.9	0.90
$(PEABr)_{1.0}CsPbBr_3$	513	71.8	25.1	0.92

Table 1. Photoluminescence quantum yield, PL peak, full width half maxima and PL stability (irradiance 93 mW/ cm^2 ; λ_{exc} = 405 nm) for all different compositions of $(PEABr)_xCsPbBr_3$ used in this study. All films were on glass and encapsulated in an N_2 filled glovebox.

We now proceed to incorporate the films into LEDs to assess the effect of PEABr on both device performance, and critically, upon device stability. In this work, we use a *p-i-n* device architecture of ITO/poly-TPD/LiF/$(PEABr)_xCsPbBr_3$/TPBi/LiF/Al, a schematic of which we show in Fig. 2a, along with an energy level diagram for individual isolated materials employed in the LED stack in Fig. S4. We characterise the current density (J) *versus* external electroluminescent quantum efficiency (EQE_{EL}), current-density-voltage-luminance (J-V-L) characteristics and show device statistics in Figs. 2 b-d and EQE_{EL} *versus* luminance in Fig. S5. The maximum EQE_{EL} achieved for each composition and other performance metrics are summarised in Table 2. We achieve an excellent EQE_{EL} of 12.1 % for the $(PEABr)_{0.4}CsPbBr_3$ LED showing a large improvement from our $CsPbBr_3$ device that exhibits a maximum EQE_{EL} of only 0.24 %.

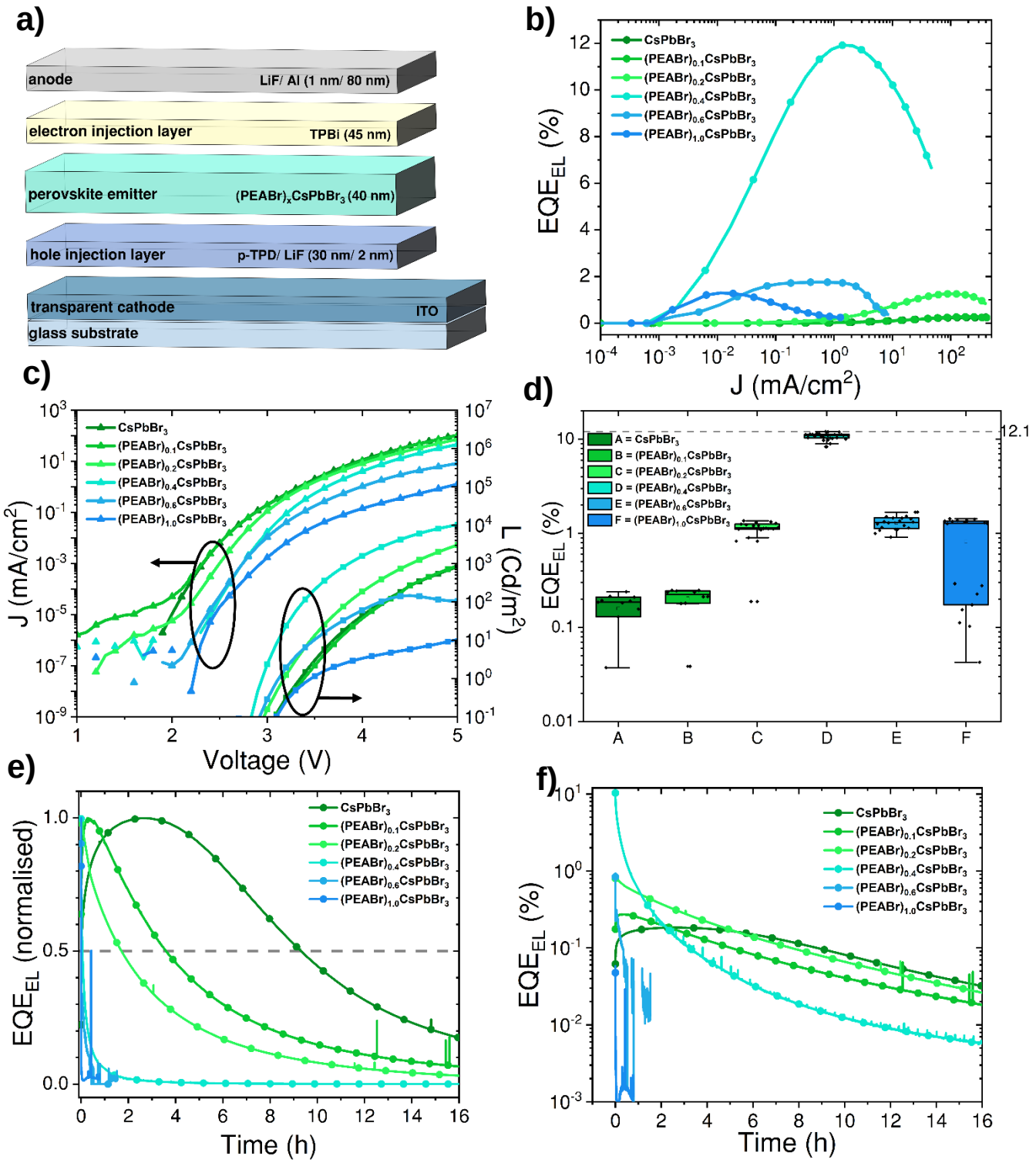

Figure 2. Device Characterisation and Stability of PEABr/$CsPbBr_3$ Perovskite LEDs: a) Device structure of LED used for this study with corresponding film thicknesses; b) Typical EQE_{EL} v current density scans for each composition; c) Current density v Voltage and Luminance v Voltage scans for the same devices; d) EQE_{EL} statistics for one batch of

perovskite LEDs across the different compositions; e) Normalised EQE_{EL} v Time data for perovskite LEDs operated at 10 mA cm^{-2} showing the drop off in stability when PEABr excess is increased; f) The same stability data plotted on an absolute scale showing that our most efficient LEDs become worse than the controls after ~ 2 hours.

It is interesting to note that the trend of PLQY does not closely follow the trend of EQE_{EL}. For $(PEABr)_{0.1}CsPbBr_3$ and $(PEABr)_{0.2}CsPbBr_3$ we saw significant improvement in PLQY but the EQE_{EL} shows no improvement for $(PEABr)_{0.1}CsPbBr_3$ and only moderate improvement for $(PEABr)_{0.2}CsPbBr_3$, in comparison to the neat CsPbBr3 LEDs. A reduction in EQE_{EL} can arise from a reduction in the emission efficiency (PLQY) of the isolated emitter layer, luminescence quenching *via* the presence of charge injection contacts, or unfavourable charge balance. If we specifically compare $(PEABr)_{0.4}CsPbBr_3$ to $(PEABr)_{1.0}$ $CsPbBr_3$, we observe a sizeable increase in PLQY of the isolated thin films (Table 1), but a substantial drop in EQE_{EL}. This tells us that either the luminescence quenching from the charge extraction contacts is sensitive to the emission layer composition, or that the charge balance has become less favourable. We will return to this point when investigating the operational stability of the devices later on.

Interestingly, despite a high peak EQE_{EL}, this does roll off at higher drive voltages, and $(PEABr)_{0.6}CsPbBr_3$ and $(PEABr)_{1.0}CsPbBr_3$ achieve a maximum luminance of only 145 and 11 cd/ m^2 respectively which is presently too low for commercial use (typically OLEDs operate up to 1000 cd/m^2). In Fig. 2c with increasing amount of PEABr we observe a significant decrease in current for a given voltage. PEABr is an insulating organic molecule and is expected to decrease the conductivity of the film; it is logical that there will be an optimal amount for high efficiency LEDs where a trade-off between electronic conductivity and improvement in PLQY of the film on injecting contacts is achieved.

Next, we investigate the operational stability of the devices in a nitrogen filled glovebox, to remove the effects of atmosphere upon stability. We operate devices at a constant current

density of 10 mA cm^{-2} and measure the EQE_{EL} as a function of time. We present the results both normalised to their maximum values and on an absolute scale (Fig. 2e and 2f, respectively). Strikingly, as we increase the PEABr content from $CsPbBr_3$ → $(PEABr)_{1.0}CsPbBr_3$, we see a strong negative correlation with stability, and we determine that the T_{50} decreases from 9.3 hours to a few seconds (Table 2, Fig. S6). Most worrying is T_{50} for $(PEABr)_{0.4}CsPbBr_3$, our most efficient LED is only 203 seconds, over 150 times shorter than our control $CsPbBr_3$ device. After further inspection of Fig. 2 f one can see that $(PEABr)_{0.4}CsPbBr_3$ becomes less efficient than $CsPbBr_3$ after only 2.5 hours, which raises concerns for PEABr addition as a strategy for fabricating efficient perovskite LEDs.

Perovskite Composition	**Max EQE_{EL} (%)**	**T_{50} @ 10 mA cm^{-2}**	**Maximum Luminance (cd m^{-2})**	**Turn-on voltage (V)**	**J @ max EQE_{EL} (mA cm^{-2})**	**Luminance @ max EQE_{EL} (cd m^{-2})**	**EL peak (nm)**
$CsPbBr_3$	0.24	9.3 h	3495	3.0	413	3496	523
$(PEABr)_{0.1}CsPbBr_3$	0.25	3.6 h	3366	3.0	178	1611	521
$(PEABr)_{0.2}CsPbBr_3$	1.38	1.7 h	10973	2.9	106	4426	516
$(PEABr)_{0.4}CsPbBr_3$	12.1	203 s	10270	2.8	2	812	514
$(PEABr)_{0.6}CsPbBr_3$	1.68	3 s	146	2.8	0.4	32	509
$(PEABr)_{1.0}CsPbBr_3$	1.43	6 s	10	3.0	0.02	1	509

Table 2. Max EQE_{EL} achieved, T_{50} at 10 mA cm^{-2} and other performance metrics for all $(PEABr)_xCsPbBr_3$ LEDs measured in this study.

Having discovered this striking trend, we reviewed the literature of $CsPbBr_3$ LEDs (using *p-i-n* device structures) to see if there is general consistency. We categorise the different reports of LEDs under three general strategies: these are (i) bulk $CsPbBr_3$ with polymers or small molecules for passivation (*e.g.* polyethylene oxide[21] or cesium trifluoroacetate[22]), (ii) $CsPbBr_3$ with bulky ammonium cations, and (iii) colloidal nanocrystals of $CsPbBr_3$ (see table S2 for review), which employ a range of ligands for passivation. It isn't possible to make absolute

stability comparisons across studies since different operational conditions have been used, however we observe that the T_{50} for bulk $CsPbBr_3$ is superior to $CsPbBr_3$ with bulky ammonium additives and $CsPbBr_3$ nanocrystals. Additionally, the two best reported stabilities which we can find for green perovskite LEDs, are derived from bulk $CsPbBr_3$ with impressive T_{82} = 80 h and T_{50} = 250 h while maintaining an efficiency of 4.8 % and 10.5 % respectively.[21,22] The literature is therefore consistent with our findings that ammonium cations are detrimental to the stability of $CsPbBr_3$ LEDs.

We now seek to unveil the underlying degradation mechanism in PEABr-containing $CsPbBr_3$ LEDs. We first consider the thermal stability of our $(PEABr)_{0.4}CsPbBr_3$ LEDs. $CsPbBr_3$ is well known to be thermally stable[15] and previous reports for $(PEABr)_{0.4}CsPbBr_3$ have shown optimised annealing times of 10 minutes at 90 ºC after which a thermally induced degradation in optoelectronic properties is observed.[23] Jiang *et al.* recently reported high efficiency perovskite solar cells where they used PEAI as a surface passivation treatment and they found that their treatment was unstable at 85 °C.[24] Therefore, we anneal $(PEABr)_{0.4}CsPbBr_3$ LEDs at 50 °C and measure the efficiency over the course of an hour to check if thermal decomposition is occurring (Fig. 3b.). We choose this temperature since Zhao *et al.* measured the junction temperature of their perovskite LEDs (which have a very similar emitter and device structure to ours) in operation to be approximately 40 °C.[19] We observe no change in efficiency over the course of one hour, which rules out operationally induced thermal degradation as the sole mechanism. We also measure the photostability of the films under illumination at 93 mW/cm^2 (Fig. S7). We firstly observe that none of the films degrade by anywhere near the same extent as the $(PEABr)_{0.4}CsPbBr_3$ LEDs over the same period of time, and that the trend in stability does not follow closely with the LEDs: the $(PEABr)_{0.2}CsPbBr_3$ has the lowest photostability.

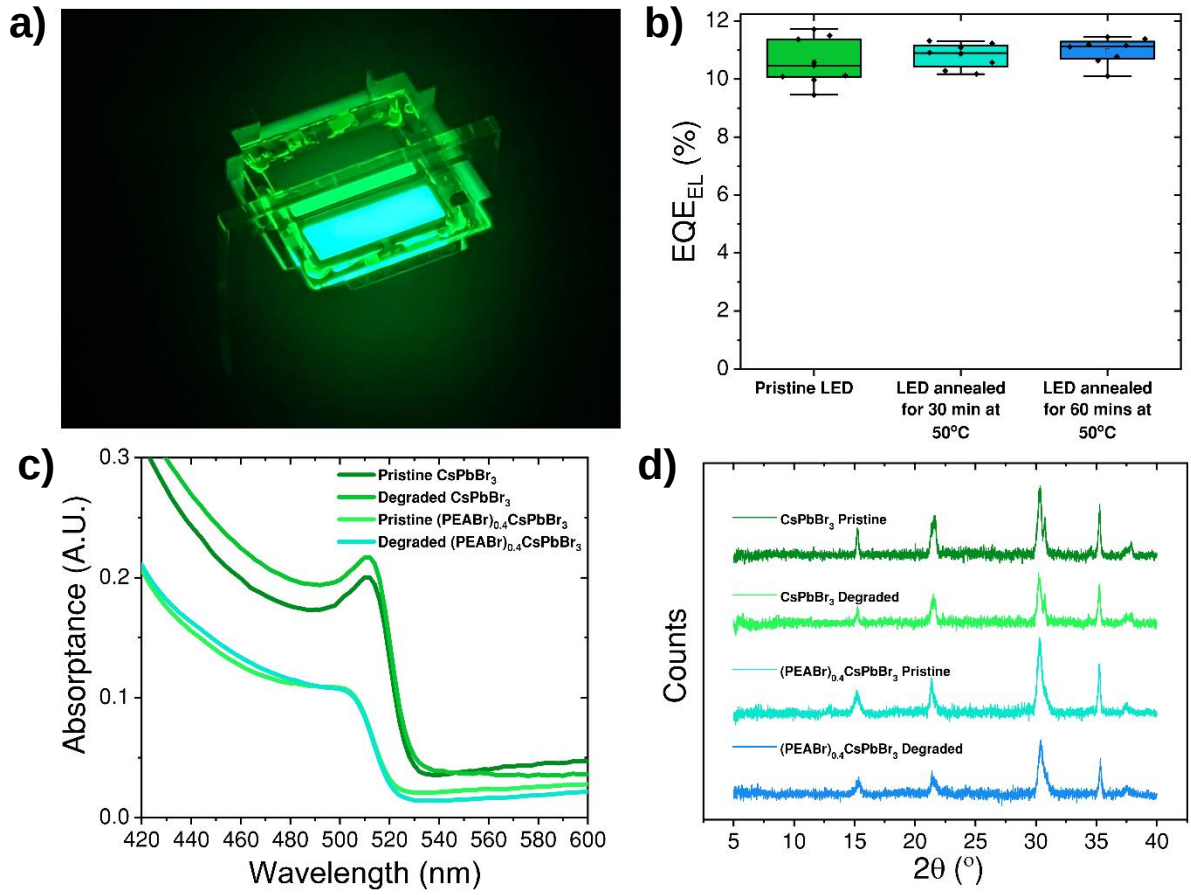

Figure 3. Characterisation of Degraded Perovskite LEDs: a) A 1 cm^2 $(PEABr)_{0.4}CsPbBr_3$ LED in operation which was typically used to maximise signal when characterising degradation; b) EQE_{EL} statistics for all 8 pixels on one $(PEABr)_{0.4}CsPbBr_3$ substrate after annealing for different periods of time at 50 ˚C; c) UV-Visible absorptance data for pristine and degraded LEDs, typically 2 x 1 cm^2 electrodes were evaporated on a substrate, one was electrically degraded and both the electrodes were delaminated for further characterisation; d) XRD data for LEDs where the same degradation procedure as for the UV-Vis was carried out.

To further elucidate the degradation mechanism, we probe the electronic and crystal structure of our $CsPbBr_3$ and $(PEABr)_{0.4}CsPbBr_3$ LEDs before and after operation. In order to maximise signal and degradation we use 1 cm^2 devices, which we show in operation in Fig. 3a., and

operate them at 20 mA cm^{-2} for 1 hour. We present the UV-Vis and XRD data (Fig. 3c, d). Surprisingly, despite almost complete degradation of the EQE_{EL} for $(PEABr)_{0.4}CsPbBr_3$ LEDs, we do not see any changes in the XRD or UV-Vis. Further, we consider whether changes in morphology are occurring so we operate the LEDs, delaminate the Al electrode, wash off the TPBi top contact with chlorobenzene, and then characterise the top of the perovskite film using SEM (Fig. S8). We observe no significant changes in morphology which is consistent with the lack of changes in the XRD and UV-Vis. X-ray photoelectron spectroscopy (XPS) is performed on the same samples, and again, we observe no significant changes in the Pb 4*f*, Al *2p* or Br 3*d* core level spectra. Full peak fittings, positions and data comparisons can be found in figures S9-11 and Table S4.

Next, we measure the photoluminescence spectra of our pristine and degraded $(PEABr)_{1.0}CsPbBr_3$ LEDs and observe a slight redshift in the spectrum (Fig. S12 a). This is consistent with an increase in the $CsPbBr_3$ domain size, which would reduce the confinement of the carriers. We postulate that the apparent loss of confinement is due to phenylethylammonium decomposing in our $(PEABr)_{1.0}CsPbBr_3$ LEDs *via* the reaction:

$$R\text{-}NH_3^+X^- \rightarrow R\text{-}NH_3 + HX$$

Equation 1. Proposed decomposition pathway for PEABr where R = C_6H_5-CH_2-CH_2 and X = Br^- which is analogous to the well know decomposition reaction of methylammonium iodide where R = CH_3 and X = I^-

Where R = C_6H_5-CH_2-CH_2 and X = Br^-. This decomposition reaction is analogous to the decomposition of methylammonium iodide which is well known in perovskite photovoltaics (R = CH_3 and X = I^-) which has been studied extensively, and is known to happen under environmental stresses such as elevated temperature, humidity and the presence of oxygen.[3] Indeed, Prakasam *et al.* recently investigated the degradation of methylammonium lead

bromide perovskite LEDs, and report the formation of $PbBr_2$ under operation, and show compelling evidence for the formation of methylamine, consistent with methylammonium deprotonating under electrical injection.[25] Watanabe *et al*. studied the degradation of $PEA_2FA_2Pb_3Br_{10}$ and showed degradation of their 2D phases into 3D $FAPbBr_3$.[26] They do not provide a mechanism but we postulate that they are also observing the decomposition of phenylethylammonium into phenylethylamine. Further, Fang *et al.* showed the photodecomposition of the layered perovskite PEA_2PbI_4 into PEA, HI and PbI_2 which indicates that these materials may not be stable when full of charge under electrical bias. [27]

We do not observe the same red shift in the photoluminescence spectrum of our $(PEABr)_{0.4}CsPbBr_3$ LEDs after degradation (Fig.S12 b) so we investigate them further. We study $(PEABr)_{0.4}CsPbBr_3$ LEDs at different stages of degradation using Fourier transform photocurrent spectroscopy (FTPS) under high gain settings to look for the presence of sub-bandgap states which would be contributing to photocurrent. FTPS affords orders of magnitude of sensitivity in comparison with linear absorption. However, we didn't observe the formation of a low bandgap minority phase or a low energy tail (Fig. S13). It is worth noting that while the FTPS spectrum does not change in overall shape, it does reveal a lower collected photocurrent after the LEDs have been operated. This is an indication of interfacial degradation in the device reducing the efficiency of carrier collection. It does not however indicate increased contact between the 3D domains and the charge injection layers, which could have otherwise been potentially responsible for the reduced EQE_{EL}.

Looking further for an indication of decomposition we closely inspect the spectral features of the electroluminescence (EL) of $(PEABr)_{0.4}CsPbBr_3$ LEDs over the course of degradation. Fig. S14 a shows the decrease of EL intensity over the course of the measurement with the normalised spectra shown in the inset. First, it appears that there was no significant change in the spectrum. However, when shown on a log scale, we find a broad shoulder spanning from

600-900 nm growing relative to the 520 nm emission over the course of time (Fig. S14 b). Intrigued by the presence of this shoulder we look at the same region for $CsPbBr_3$ LEDs (Fig. S14 d), and observe that even the pristine LED has a broad shoulder between 600-900 nm. Interestingly, this shoulder grows at a much slower rate than in the $(PEABr)_{0.4}CsPbBr_3$ LEDs, which correlates with our observations for stability. This type of broad emission in $CsPbBr_3$ was first reported by Motti *et al.* under PL excitation in vacuum which they attributed to photo-emissive trap states.[28] As far as we are aware this is the first report of such emissive trap states in EL, and may provide a compelling signature of the degradation of our films.

We continue our investigation by probing the electrical characteristics of our $(PEABr)_{0.4}CsPbBr_3$ LED before and after significant amounts of degradation (1 h operation at 10 mA cm^{-2}). We find that for a given current density the luminance is approximately 2 orders of magnitude lower for the degraded device (Fig. 4 a). We observe that there is an increase in current density at low bias (Fig 4 b), indicating either (i) a reduction in the shunt resistance (leakage current), (ii) an increase in the background carrier density in the perovskite films or (iii) doping of the injection layers. However, when we reach the turn on voltage for the LED (~2.8 V) less current is flowing through the device. The increased resistance under operating conditions could result from either a reduction in charge carrier mobility in the perovskite emitter layer or in the charge injection layers, or an increased barrier to charge injection at one or both of the contacts. This change to the resistance and current flow through the LED is likely to have a negative impact on efficiency. If the charge injection is primarily limited for one carrier type (electron or holes), then there may exist a unipolar current of the opposite carrier type, where the charges then drift right through the device and back into the external circuit.[29] A significant charge injection barrier can also lead to the opposite carrier accumulation at that interface, leading to increased non-radiative recombination in the electrodes, transport materials or at this interface. Upon further inspection of Fig. 4 b one can see that the turn-on

voltage has increased by 0.3 V to ~3.1 V in the degraded device. This is in agreement with the observed 'kink' in the JV curve (which is related to the built-in voltage) which increases from 2.6 V to 2.9 V. The determination of the physical origin of this barrier and its location in the device is the subject of ongoing work.

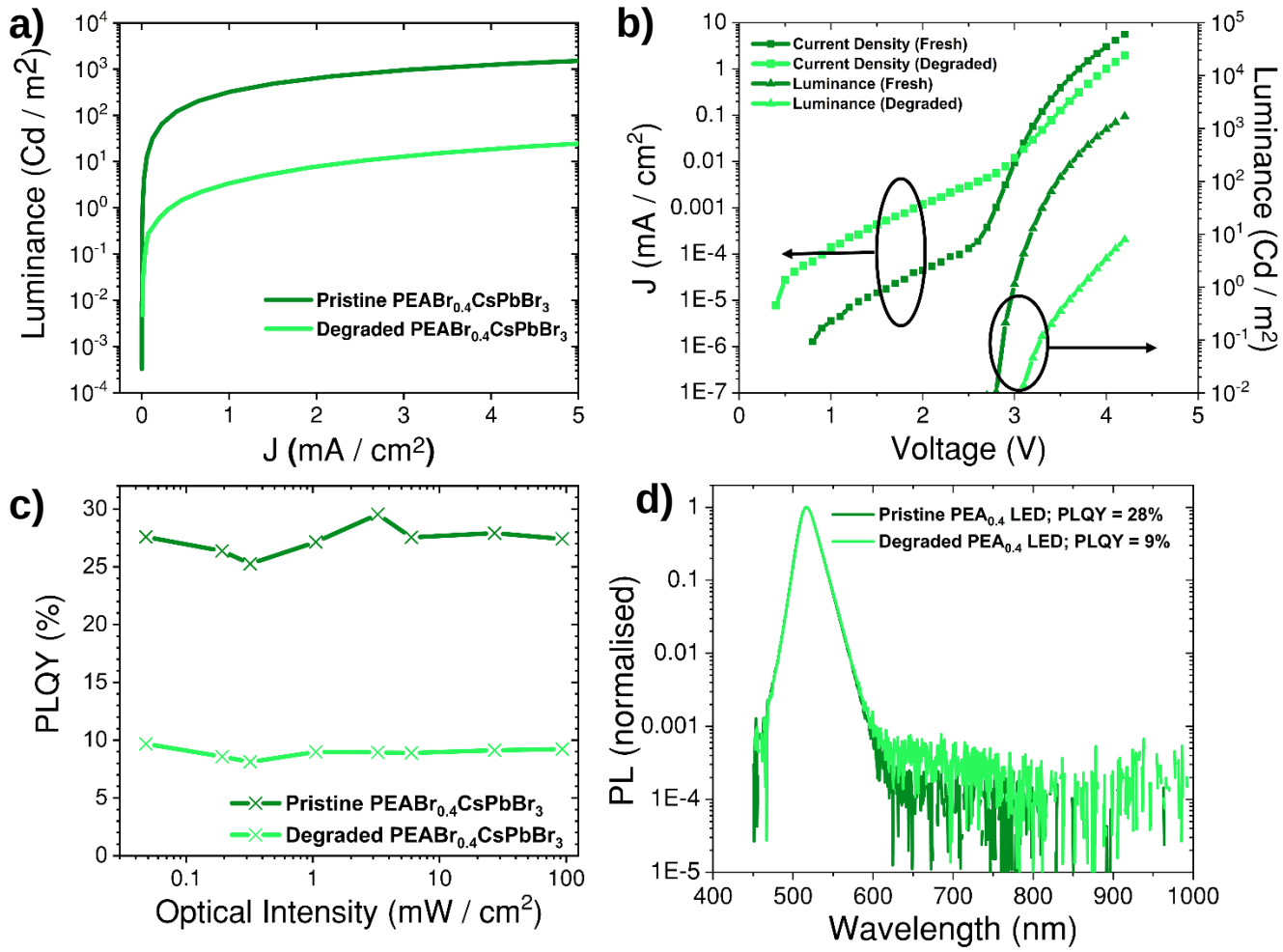

Figure 4: Changes in electronic and optoelectronic characteristics of $(PEABr)_{0.4}CsPbBr_3$ LEDs after degradation, this LED had an initial EQE_{EL} of 10.3%: a) J v L of pristine and degraded LED after 1 h of operation at 10 mA cm^{-2} ; b) changes in J-V-L characteristics before and after 1 h of operation at 10 mA cm^{-2} ; c) intensity dependence of PLQY of full LED before and after

operation for 1 h at 10 mA cm^{-2} ; d) changes in the PL spectrum of $(PEABr)_{0.4}CsPbBr_3$ LED after operation for 1 hour at 10 mA cm^{-2}

Next we measure the PLQY of our full device stack for the same $(PEABr)_{0.4}CsPbBr_3$ LED for which we have just presented the JVL data, before and after operation. We find that the PLQY decreases from ~28% down to ~9% across a wide range of optical excitation intensities (Fig. 4 c). In addition to the decrease in PLQY, we also observe the previously mentioned tail in the emission of degraded $(PEABr)_{0.4}CsPbBr_3$ (Fig. 4 d). Interestingly, the PLQY of the degraded devices is much higher than the degraded EQE_{EL} and experiences much less of a relative decrease, only dropping to ~30% of its initial value whereas the EQE_{EL} is ~1.5% of its initial value. It therefore appears that although a certain fraction of the degradation in EQE_{EL} is originating from trap site generation in the perovskite emission layer, the majority of the degradation is arising from an electronic consequence of the increased resistance under driving voltages.

We also note that even before degradation, the PLQY of the complete device (metal electrodes included) is much higher than the EQE_{EL} that we determine. This shows that there are electronic losses under operation which are not present under light illumination. This indicates that the charge injection layers are not perfect charge blocking when an electric field is applied, or that there is an imbalance in the charge injection rate for electrons and holes, and clearly indicates significant scope for improvement of the LEDs. Further, we note that the PLQY does not vary with optical excitation intensity even for the degraded LED we present. If we are creating traps in the bulk of the emission layer in the degraded devices, we would expect lower PLQE at low excitation intensities, due to trap filling with increasing excitation

intensity. Since we do not observe this, we postulate that the non-radiative recombination is happening mostly at the interfaces.

In this work we show that the addition of PEABr to $CsPbBr_3$ perovskite LEDs significantly decreases the operational stability. The T_{50} = 9 hours for $CsPbBr_3$ which we report is over 2 orders of magnitude longer than our high efficiency $(PEABr)_{0.4}CsPbBr_3$ LEDs. However, we do not find any significant changes to the electronic or crystal structure of the material after degradation. We do observe that the PLQY of our optimised device decreases from ~28% to ~9% after 1 hour of operation at 10 mA cm^{-2} (32% its initial value), but this does not fully explain the drop in EQE_{EL} which drops from 10.3% to 0.16% during this time (1.5% its initial value). Additionally, we observe significant changes in the J-V characteristics of the device over this time. Namely, we observe an increase in current density below the LED turn on voltage and a reduction in the current density, hence increase in resistance, above the turn on voltage.

It is apparent that the primary cause for the rapid degradation are changes to the electronic operating characteristics of the devices, rather than changes to the emission efficiency of the emitter layer. Metal halide perovskites are known to contain mobile ions, which can have significant effects on the electronic characteristics of devices.[30,31] We postulate that the changes we observe are a result of an alteration of the charge injection contacts as a consequence of mobile ions migrating from the perovskite emitting layer into the charge injection layers, or accumulating at one of the interfaces in the device. Due to the direction of the electric field under operation, we would expect diffusive cations to be driven into the *n*-type charge injection interface and layer (cathode), and anions to be driven into the *p*-type charge injection layer and interfaces (anode). Depending upon the precise nature of the ions, this accumulation of ions could result in increased *n*- or *p*-doping of the respective injection layers, in an analogous

fashion to a light emitting electrochemical cell.[32] Further, a significant shift in the energetic alignment could occur at these interfaces due to dipole layer formation or the accumulation of a solid-state ionic double layer. Both these processes could significantly influence the charge injection and recombination at these interfaces.

The clear trend of decreasing operational stability with increasing concentration of PEABr, points towards it being a likely source of these mobile ions. As we previously highlighted (Equation 1), there is evidence in the literature for generation of HBr in operating devices *via* decomposition of alkylammonium halides. We postulate that the H^+ and Br^- ions formed are the previously mentioned mobile ions. $CsPbBr_3$ does not contain any alkylammonium cations so cannot undergo the same decomposition pathway, which can explain the relative increase in stability. However, it does contain mobile ions (mainly interstitials and vacancies)[31] which may still play a role on the long term stability. Analysis of changes in ion distributions before and after operation of perovskite LEDs should be critical in further elucidating degradation processes, and identifying means to circumvent such degradation. There is evidence in the literature of ion migration through the device, a recent analysis on degraded $FAPbI_3$ LEDs through time of flight- secondary ion mass spectrometry shows accumulation of I^- at the TFB (*p*-type) / Au interface.[33] Understanding these processes in more depth, is subject to ongoing work.

The decreased PLQY in the devices indicated enhanced non-radiative recombination. This could be explained by (i) the decomposition of PEABr reducing chemical passivation in the film, (ii) doping of the contact layers by mobile ions increasing interfacial non-radiative recombination, or (iii) the formation of other unidentified traps during operation. We wish to stress that it is not clear from our characterisation which one of these contributes to the loss in PLQY, therefore we believe that further research is required to determine if this loss can be prevented in these hybrid materials.

We consider that the capability of perovskite LEDs has been well demonstrated by the field and now stability should be more critically assessed. In light of our findings we propose that future research into the stability of perovskite LEDs should focus on (i) the development of new charge injection layers and device architectures which are impervious to the diffusion of mobile ions, and (ii) the development of perovskite materials which have less diffusive ions while maintaining high luminescence efficiency. It appears that $CsPbBr_3$ is a good material for further investigation since it does not contain labile protons which can dissociate.

Conclusions

In conclusion, we have found that phenylethylammonium bromide is extremely beneficial for improving the efficiency of $CsPbBr_3$ LEDs, whereby we are able to improve the EQE_{EL} 50 fold from 0.24 % for $CsPbBr_3$ up to 12.1 % for $(PEABr)_{0.4}CsPbBr_3$. This is in agreement with the literature, where PEABr has been widely used to achieve this goal. However, we have found a very strong negative correlation between incorporation of PEABr and operational stability. After careful characterisation of degraded LEDs, we attribute the decay of the efficiency in part to an increased trap density in the emissive layer, but also and most significantly, to a negative impact upon the charge injection and transport characteristics in the electrically-driven LED. We postulate that the most prominent cause for these effects is the decomposition of PEABr into phenylethylamine and HBr. This reaction generates mobile ions, which can drift towards the charge injection interfaces, which could have a broad range of negative consequences. This has not been previously observed or considered for perovskite LEDs and provides a new direction for addressing these challenges by engineering improved contacts which are either insensitive or impermeable to ionic species. However, when we compare the stability of different $CsPbBr_3$ perovskite LEDs from our results and literature, we find that bulk $CsPbBr_3$

is a superior material for stability. We believe that, further research into methods to improve the efficiency and stability of bulk $CsPbBr_3$ LEDs, coupled with redesigning the charge injection layers will yield a significant step towards achieving respectable operational stabilities for perovskite LEDs.

Methods

Materials

Lead(II) bromide 99.999% (35703, Alfa Aesar), Cesium bromide 99.999% (429392, Sigma Aldrich), 18-crown-6 ≥99.0% (274984, Sigma Aldrich), poly-tpd (PE0299, 1-Material Inc.), TPBi (LT-E302, Lumtec Inc.), LiF (LT-E001, Lumtec Inc.), Phenylethylamine (128945, Sigma Aldrich), Ethanol (443611, Sigma Aldrich), Dimethyl sulfoxide (276855, Sigma Aldrich) and Chlorobenzene (284513, Sigma Aldrich) were all used as purchased without further purification.

PEABr was prepared by the following procedure; 5 mL of phenethylamine and 30 mL of ethanol were mixed and stirred in a 250 mL 2-neck flask in an ice-water bath. Then, 6.8 mL of HBr acid (48 wt% in water) was slowly added into the mixture. The mixture was stirred for 2 h at 0 °C maintained using an ice-water bath. The reacted solution was evaporated by a rotary evaporator at 55-60 °C to remove the solvent (ethanol and water), and white precipitate was formed. The white precipitate was then washed with diethyl ether and collected by vacuum filtration, a step which was repeated three times. After filtration, the obtained PEABr white powder was collected and dried in a vacuum oven at 60 °C overnight. After that, PEABr was dissolved into ethanol and diethyl ether to obtain a supersaturated solution. The solution was

put into a freezer overnight. The white precipitate was then washed with diethyl ether and collected by vacuum filtration, a step which was repeated three times. After filtration, the obtained PEABr white powder was collected and dried in a vacuum oven at 60 °C overnight. It was then transferred to an N_2 glovebox

Perovskite film fabrication

Perovskite precursor solutions were prepared to a standard wt % of approximately 12.4% where our $(PEABr)_{0.4}CsPbBr_3$ samples were at a concentration of 0.2 M; The masses in mg / mL of all of the salts for the solutions can be found in Table S1. All of the following procedures were carried out in a N_2 filled glovebox. The solutions were prepared by weighing all of the powders into a single vial, dissolving them in anhydrous DMSO by stirring at 50 °C for 3 hours and then filtering with a 0.45 μM PTFE membrane filter. A spincoating program of 1000 rpm (1000 rpm s^{-1} ramp) for 5 s followed by 3000 rpm for 55 s (3000 rpm s^{-1} ramp) was used. The spincoater was set up with a plastic collar (15 cm diameter) lined with a clean room wipe surrounding the chuck and run with the lid open (using a magnet to override the interlock). The 28 x 28 mm substrate was placed on the chuck and spun for approximately 2 s before 50 uL of precursor solution was dynamically dispensed onto the spinning substrate. We periodically checked the substrate while it was spinning with a UV torch to check for luminescence and found the $(PEABr)_{0.4}CsPbBr_3$ samples to begin to luminesce approximately 30 s into the spin program. The film was then annealed for 10 minutes at 100 °C; we observed that for $(PEABr)_{0.4}CsPbBr_3$ the luminescence is initially quenched but returns visibly to its initial intensity after 5 minutes. After each film was spincoated the clean room wipe was replaced in order to reduce the amount of DMSO in the immediate vicinity of the film during crystallisation. We found this critical for the fabrication of reproducible films and devices.

LED fabrication

Pre-etched 28 x 28 mm ITO substrates were cleaned by sonication in a 2 v/v% Decon 90 detergent solution, deionised water, acetone and isopropanol for 2 minutes each. The substrates were dried with a stream of N_2 and cleaned by UV-Ozone for 10 minutes. Then a solution of poly-tpd in chlorobenzene (5 mg/mL) was dynamically spincoated in ambient air onto the substrates at 4000 rpm for 20 s.

The substrates were then transferred to a vacuum evaporation chamber contained in a N_2 filled glovebox and pumped down to a pressure of 5 x 10^{-6} mbar before 2 nm LiF was evaporated (rate = 0.1 A s^{-1}) over the entire area of the substrate. The LiF helps to improve the wettability of the perovskite on the poly-tpd while also reducing interfacial recombination. The samples were kept in a N_2 environment in order to prevent the adsorption of water to the surface as LiF is hygroscopic. Subsequently the perovskite film was deposited as described in the above section, it is worth reiterating that the perovskite solution is dynamically dispensed onto the already spinning substrate 2 seconds into the program. The substrates were then transferred to a vaccum evaporation chamber without exposure to air and pumped down to 5 x 10^{-6} mbar. 45 nm TPBi (rate 1 A s^{-1}) was evaporated from an alumina crucible followed by 1 nm LiF (rate = 0.1 A s^{-1}). These two materials were evaporated over the entire area of the substrate and the chamber was vented. They were then transferred into a different evaporation mask and placed into the chamber again where 100 nm Al (rate = 1 A s^{-1}) was evaporated from an alumina coated molybdenum boat. The mask which defined the pixel area creates an overlap area between the patterned ITO and the aluminium of 3 x 3 mm giving a total pixel area of 9 mm^2.

ELQE measurement

The ELQE was measured using two different setups to allow for cross reference of values.

ELQE using calibrated photodiode

Current density-voltage characteristics (J-V) were measured with a Keithley source-measure unit (2400 series). Simultaneously the photon flux was measured by a calibrated photodiode

(Thorlabs FDS 1010) which was placed directly above the sample at a distance of 9 mm and held in a forward bias of 3 V. The total number of photons emitted from the sample was calculated assuming a Lambertian emission profile and calculating the radiation view factor which corrects for the fact that the LED is not a point source at this distance. Details of this calculation can be found in Fig. S15. The electroluminescence spectrum was measured using a calibrated grating spectrometer (MayaPro 2000). Using these data in addition to the responsivity of the photodiode, all of the relevant performance characteristics can be calculated (details can be found here).[34] All measurements were carried out in an N_2 filled glovebox.

ELQE using an integrating sphere

Current density-voltage characteristics (J-V) were measured by Keithley source-measure unit (2400 series). The LED was placed in an N_2 filled holder which was mounted to the side of an integrating sphere, the electroluminescence spectrum and the photon flux was simultaneously measured using a calibrated grating spectrometer (MayaPro 2000). Using these data all of the relevant performance parameters can be calculated.

LED Stability testing

The LED stability was measured using the calibrated photodiode ELQE setup mentioned above. The El spectrum was first measured using a calibrated grating spectrometer (MayaPro 2000). A constant current density of 10 mA cm^{-2} was applied and the photodiode current was measured as a function of time, from this the ELQE as a function of time was calculated.

PLQY, Steady state PL and EL spectra

Photoluminescent quantum efficiency measurements were carried out using a 405 nm laser (Roithner laser MLL-III-405-200mW) an integrating sphere and a calibrated grating spectrometer (MayaPro 2000 or Maya QE Pro), using previously established protocols.[35]

Preparation of samples for degradation comparison

Samples were fabricated as described in the procedure above except a 1 cm^2 Al electrode was evaporated in the final step. After operation the electrode was delaminated using sticky tape for XRD and UV-Vis measurements. For PLQY measurements, the perovskite outside of the electrode area was scraped off. Additionally, for SEM the TPBi top contact was spin rinsed at 3000 rpm twice with 500 uL of chlorobenzene.

UV-Vis

Transmission and reflection measurements were carried out with a Perkin-Elmer 1050+ UV-Vis-NIR Spectrophotometer with an integrating sphere accessory.

SEM

The SEM micrographs were measured using a FEI Quanta 600 FEG scanning electron microscope. All of the films were imaged on an ITO/ Poly-TPD / LiF substrate.

XPS

A Thermo Scientifc Ka X-Ray Photoelectron spectrometer was used to perform XPS measurements using a monochromated Al Ka X-Ray source at a take-off angle of 90°. The core level XPS spectra were recorded using a pass energy of 20 eV (resolution approximately 0.4 eV) from an analysis area of 300 μm x 300 μm. The spectrometer work function and binding energy scale were calibrated using the Fermi edge and 3d peak recorded from a polycrystalline silver (Ag) sample prior to the commencement of the experiments. Fitting procedures to extract peak positions and relative stoichiometry from the XPS data were carried out using CASA XPS software suite

XRD

XRD diffractograms were obtained using a Panalytical X'Pert Pro X-Ray diffractometer with a Cu-alpha source ($\lambda = 1.54$ Å).

FTPS

The photovoltaic external quantum efficiency (EQE_{PV}) was measured using a custom-built Fourier transform photocurrent spectrometer based on a Bruker Vertex 80v Fourier transform interferometer. Devices were illuminated with a 0.4 sun (40 mW/cm^2), AM 1.5G spectrum generated by an Oriel class AAA solar simulator. The LEDs were masked with a metal aperture, with a defined active area of 0.0625 cm^2. All of the photocurrent measurements were carried out in air. To calculate the EQE_{PV}, the device photocurrent spectrum was divided by a calibrated silicon reference cell spectrum with a known EQE. The acquisition time for each spectrum was approximately 1 min.

Supplementary Information

The Supplementary information is available online free of charge at:

Additional notes on the broadening of the emission and absorption of quantum confined perovskites; A literature review of stability of $CsPbBr_3$ LEDs; tabulated concentration of precursors used to fabricate films, tabulated initial and peak luminances of LEDs under steady state operation at 10 mA cm^{-2}; Energy level diagram of $CsPbBr_3$ LEDs; Figures showing pristine film morphology, X-ray diffraction, EQE_{EL} v Luminance, photostability, changes in PL and EL spectra after device operation, changes in morphology after operation, XPS data and fits, FTPS data, a script for calculation of radiation view factors.

Acknowledgements

J.H.W. acknowledges the Engineering and Physical Sciences Research Council (EPSRC) and Centre for Doctoral Training in New and Sustainable Photovoltaics for financial support.

A.J.R., H.C.S. and H.J.S. acknowledge the EPSRC for funding; grant numbers EP/ M005143/1, EP/S004947/1 and EP/M015254/1. A.J.M acknowledges the Strategic University Network to Revolutionise Indian Solar Energy (SUNRISE) for funding. R.D.J.O. gratefully acknowledges the Penrose Scholarship for funding. B.W. acknowledges funding from the European Union's Horizon 2020 research and innovation programme under Grant Agreement No. 763977.

References

(1) Best Research-Cell Efficiency Chart, https://www.nrel.gov/pv/assets/pdfs/best-research-cell-efficiencies.20200406.pdf. (accessed June 18th 2020)

(2) Lee, M. M.; Teuscher, J.; Miyasaka, T.; Murakami, T. N.; Snaith, H. J. Efficient Hybrid Solar Cells Based on Meso-Superstructured Organometal Halide Perovskites. *Science.* **2012**, *338*, 643–647.

(3) Grancini, G.; Roldán-Carmona, C.; Zimmermann, I.; Mosconi, E.; Lee, X.; Martineau, D.; Narbey, S.; Oswald, F.; De Angelis, F.; Graetzel, M.; Nazeeruddin, M. K. One-Year Stable Perovskite Solar Cells by 2D/3D Interface Engineering. *Nat. Commun.* **2017**, *8*, 15684.

(4) Tan, Z.-K.; Moghaddam, R. S.; Lai, M. L.; Docampo, P.; Higler, R.; Deschler, F.; Price, M.; Sadhanala, A.; Pazos, L. M.; Credgington, D.; Hanusch, F.; Bein, T.; Snaith, H. J.; Friend, R. H. Bright Light-Emitting Diodes Based on Organometal Halide Perovskite. *Nat. Nanotechnol.* **2014**, *9*, 687–692.

(5) Lu, M.; Zhang, Y.; Wang, S.; Guo, J.; Yu, W. W.; Rogach, A. L. Metal Halide Perovskite Light-Emitting Devices: Promising Technology for Next-Generation Displays. *Adv. Funct. Mater.* **2019**, *29*, 1902008.

(6) Cao, Y.; Wang, N.; Tian, H.; Guo, J.; Wei, Y.; Chen, H.; Miao, Y.; Zou, W.; Pan, K.; He, Y.; Cao, H.; Ke, Y.; Xu, M.; Wang, Y.; Yang, M.; Du, K.; Fu, Z.; Kong, D.; Dai, D.; Jin, Y.; Li, G.; Li, H.; Peng, Q.; Wang, J.; Huang, W. Perovskite Light-Emitting Diodes Based on Spontaneously Formed Submicrometre-Scale Structures. *Nature* **2018**, *562*, 249–253.

(7) Lin, K.; Xing, J.; Quan, L. N.; de Arquer, F. P. G.; Gong, X.; Lu, J.; Xie, L.; Zhao, W.; Zhang, D.; Yan, C.; Li, W.; Liu, X.; Lu, Y.; Kirman, J.; Sargent, E. H.; Xiong, Q.; Wei, Z. Perovskite Light-Emitting Diodes with External Quantum Efficiency Exceeding 20 per Cent. *Nature*. **2018**, *562*, 245–248.

(8) Zhao, B.; Bai, S.; Kim, V.; Lamboll, R.; Shivanna, R.; Auras, F.; Richter, J. M.; Yang, L.; Dai, L.; Alsari, M.; She, X.-J.; Liang, L.; Zhang, J.; Lilliu, S.; Gao, P.; Snaith, H. J.; Wang, J.; Greenham, N. C.; Friend, R. H.; Di, D. High-Efficiency Perovskite–Polymer Bulk Heterostructure Light-Emitting Diodes. *Nat. Photonics* **2018**, *12*, 783–789.

(9) Xu, W.; Hu, Q.; Bai, S.; Bao, C.; Miao, Y.; Yuan, Z.; Borzda, T.; Barker, A. J.; Tyukalova, E.; Hu, Z.; Kawecki, M.; Wang, H.; Yan, Z.; Liu, X.; Shi, X.; Uvdal, K.; Fahlman, M.; Zhang, W.; Duchamp, M.; Liu, J. M.; Petrozza, A.; Wang, J.; Liu, L. M.; Huang, W.; Gao, F. Rational Molecular Passivation for High-Performance Perovskite Light-Emitting Diodes. *Nat. Photonics* **2019**, 13, 418–424.

(10) Xiao, Z.; Kerner, R. A.; Zhao, L.; Tran, N. L.; Lee, K. M.; Koh, T. W.; Scholes, G. D.; Rand, B. P. Efficient Perovskite Light-Emitting Diodes Featuring Nanometre-Sized Crystallites. *Nat. Photonics* **2017**, *11*, 108–115.

(11) Yang, X.; Zhang, X.; Deng, J.; Chu, Z.; Jiang, Q.; Meng, J.; Wang, P.; Zhang, L.; Yin, Z.; You, J. Efficient Green Light-Emitting Diodes Based on Quasi-Two-Dimensional Composition and Phase Engineered Perovskite with Surface Passivation. *Nat. Commun.* **2018**, *9*, 570.

(12) Xing, G.; Wu, B.; Wu, X.; Li, M.; Du, B.; Wei, Q.; Guo, J.; Yeow, E. K. L.; Sum, T. C.; Huang, W. Transcending the Slow Bimolecular Recombination in Lead-Halide Perovskites for Electroluminescence. *Nat. Commun.* **2017**, *8*, 14558.

(13) Quan, L. N.; Zhao, Y.; Garcia de Arquer, F. P.; Sabatini, R. P.; Walters, G.; Voznyy, O.; Comin, R.; Li, Y.; Fan, J. Z.; Tan, H.; Pan, J.; Yuan, M.; Bakr, O. M.; Lu, Z.-H.; Kim, D. H.; Sargent, E. H. Tailoring the Energy Landscape in Quasi-2D Halide Perovskites Enables Efficient Green Light Emission. *Nano Lett.* **2017**, 17, 3701–3709.

(14) Ban, M.; Zou, Y.; Rivett, J. P. H.; Yang, Y.; Thomas, T. H.; Tan, Y.; Song, T.; Gao, X.; Credgington, D.; Deschler, F.; Sirringhaus, H.; Sun, B. Solution-Processed Perovskite Light Emitting Diodes with Efficiency Exceeding 15% through Additive-Controlled Nanostructure Tailoring. *Nat. Commun.* **2018**, *9*, 3892.

(15) Kulbak, M.; Gupta, S.; Kedem, N.; Levine, I.; Bendikov, T.; Hodes, G.; Cahen, D. Cesium Enhances Long-Term Stability of Lead Bromide Perovskite-Based Solar Cells. *J. Phys. Chem. Lett.* **2016**, *7*, 167–172.

(16) Xing, J.; Zhao, Y.; Askerka, M.; Quan, L. N.; Gong, X.; Zhao, W.; Zhao, J.; Tan, H.; Long, G.; Gao, L.; Yang, Z.; Voznyy, O.; Tang, J.; Lu, Z.-H.; Xiong, Q.; Sargent, E. H. Color-Stable Highly Luminescent Sky-Blue Perovskite Light-Emitting Diodes. *Nat. Commun.* **2018**, *9*, 3541.

(17) Protesescu, L.; Yakunin, S.; Bodnarchuk, M. I.; Krieg, F.; Caputo, R.; Hendon, C. H.; Yang, R. X.; Walsh, A.; Kovalenko, M. V. Nanocrystals of Cesium Lead Halide Perovskites ($CsPbX_3$, X = Cl, Br, and I): Novel Optoelectronic Materials Showing Bright Emission with Wide Color Gamut. *Nano Lett.* **2015**, *15*, 3692–3696.

(18) Braly, I. L.; deQuilettes, D. W.; Pazos-Outón, L. M.; Burke, S.; Ziffer, M. E.; Ginger, D. S.; Hillhouse, H. W. Hybrid Perovskite Films Approaching the Radiative Limit with Over 90% Photoluminescence Quantum Efficiency. *Nat. Photonics* **2018**, *12*, 355–361.

(19) Zhao, L.; Lee, K. M.; Roh, K.; Khan, S. U. Z.; Rand, B. P. Improved Outcoupling

Efficiency and Stability of Perovskite Light-Emitting Diodes Using Thin Emitting Layers. *Adv. Mater.* **2019**, *31*, 1805836.

(20) Richter, J. M.; Abdi-Jalebi, M.; Sadhanala, A.; Tabachnyk, M.; Rivett, J. P. H.; Pazos-Outón, L. M.; Gödel, K. C.; Price, M.; Deschler, F.; Friend, R. H. Enhancing Photoluminescence Yields in Lead Halide Perovskites by Photon Recycling and Light out-Coupling. *Nat. Commun.* **2016**, *7*, 13941.

(21) Wu, C.; Zou, Y.; Wu, T.; Ban, M.; Pecunia, V.; Han, Y.; Liu, Q.; Song, T.; Duhm, S.; Sun, B. Improved Performance and Stability of All-Inorganic Perovskite Light-Emitting Diodes by Antisolvent Vapor Treatment. *Adv. Funct. Mater.* **2017**, *27*, 1–7.

(22) Wang, H.; Zhang, X.; Wu, Q.; Cao, F.; Yang, D.; Shang, Y.; Ning, Z.; Zhang, W.; Zheng, W.; Yan, Y.; Kershaw, S. V.; Zhang, L.; Rogach, A. L.; Yang, X. Trifluoroacetate Induced Small-Grained $CsPbBr_3$ Perovskite Films Result in Efficient and Stable Light-Emitting Devices. *Nat. Commun.* **2019**, *10*, 665.

(23) Zou, Y.; Huang, Q.; Yang, Y.; Ban, M.; Li, S.; Han, Y.; Wu, T.; Tan, Y.; Gao, X.; Song, T.; Sun, B. Efficient Perovskite Light-Emitting Diodes *via* Tuning Nanoplatelet Distribution and Crystallinity Orientation. *Adv. Mater. Interfaces* **2018**, *5*, 1801030.

(24) Jiang, Q.; Zhao, Y.; Zhang, X.; Yang, X.; Chen, Y.; Chu, Z.; Ye, Q.; Li, X.; Yin, Z.; You, J. Surface Passivation of Perovskite Film for Efficient Solar Cells. *Nat. Photonics* **2019**, *13*, 460–466.

(25) Prakasam, V.; Tordera, D.; Bolink, H. J.; Gelinck, G. Degradation Mechanisms in Organic Lead Halide Perovskite Light-Emitting Diodes. *Adv. Opt. Mater.* **2019**, *7*, 1900902.

(26) Watanabe, S.; Cheng, T.; Tumen-Ulzii, G.; Qin, C.; Matsushima, T.; Adachi, C. Excited-State Stability of Quasi-Two-Dimensional Metal Halide Perovskite Films under Optical and Electrical Excitations. *Appl. Phys. Lett.* **2019**, *115*, 233502.

(27) Fang, H.-H.; Yang, J.; Tao, S.; Adjokatse, S.; Kamminga, M. E.; Ye, J.; Blake, G. R.; Even, J.; Loi, M. A. Unravelling Light-Induced Degradation of Layered Perovskite Crystals and Design of Efficient Encapsulation for Improved Photostability. *Adv. Funct. Mater.* **2018**, *28*, 1800305.

(28) Motti, S. G.; Gandini, M.; Barker, A. J.; Ball, J. M.; Srimath Kandada, A. R.; Petrozza, A. Photoinduced Emissive Trap States in Lead Halide Perovskite Semiconductors. *ACS Energy Lett.* **2016**, *1*, 726–730.

(29) Murata, K.; Cinà, S.; Greenham, N. C. Barriers to Electron Extraction in Polymer Light-Emitting Diodes. *Appl. Phys. Lett.* **2001**, *79*, 1193–1195.

(30) Snaith, H. J.; Abate, A.; Ball, J. M.; Eperon, G. E.; Leijtens, T.; Noel, N. K.; Stranks, S. D.; Wang, J. T.-W.; Wojciechowski, K.; Zhang, W. Anomalous Hysteresis in Perovskite Solar Cells. *J. Phys. Chem. Lett.* **2014**, *5*, 1511–1515.

(31) Kim, G. Y.; Senocrate, A.; Yang, T.-Y.; Gregori, G.; Grätzel, M.; Maier, J. Large Tunable Photoeffect on Ion Conduction in Halide Perovskites and Implications for Photodecomposition. *Nat. Mater.* **2018**, *17*, 445–449.

(32) Dzwilewski, A.; Kemerink, M.; Matyba, P.; van Reenen, S.; Edman, L.; Janssen, R. A. J. A Unifying Model for the Operation of Light-Emitting Electrochemical Cells. *J. Am. Chem. Soc.* **2010**, *132*, 13776–13781.

(33) Li, N.; Song, L.; Jia, Y.; Dong, Y.; Xie, F.; Wang, L.; Tao, S.; Zhao, N. Stabilizing

Perovskite Light-Emitting Diodes by Incorporation of Binary Alkali Cations. *Adv. Mater.* **2020**, *32*, 1907786.

(34) Anaya, M.; Rand, B. P.; Holmes, R. J.; Credgington, D.; Bolink, H. J.; Friend, R. H.; Wang, J.; Greenham, N. C.; Stranks, S. D. Best Practices for Measuring Emerging Light-Emitting Diode Technologies. *Nat. Photonics* **2019**, *13*, 818–821.

(35) de Mello, J. C.; Wittmann, H. F.; Friend, R. H. An Improved Experimental Determination of External Photoluminescence Quantum Efficiency. *Adv. Mater.* **1997**, *9*, 230–232.